CrystEngComm

COMMUNICATION

View Article Online
View Journal | View Issue

Facile synthesis of hematite nanostructures with controlled hollowness and porosity and their comparative photocatalytic activities†

Cite this: *CrystEngComm*, 2014, **16**, 959

Received 19th September 2013,
Accepted 11th November 2013

DOI: 10.1039/c3ce41899e

www.rsc.org/crystengcomm

Hanfeng Liang,[a] Xun Xu,[b] Wei Chen,[a] Binbin Xu[ab] and Zhoucheng Wang*[a]

Hematite nanostructures with similar spindle-like shapes but different hollowness and porosities have been prepared by a facile hydrothermal method. The comparative photocatalytic activities of these samples were investigated and the results might be helpful to further understand the beneficial effects of hollow and porous structures.

As an important n-type semiconductor with a band gap of ~2.2 eV, hematite (α-Fe_2O_3) has been widely used as a photocatalyst in the degradation of organic pollutants and toxics.[1] However, its practical application is greatly hindered by slow charge transfer, a short hole diffusion length and a high probability of electron–hole recombination.[2] It is believed that the shape and size of materials have much influence on their chemical and physical properties.[3] Therefore, many efforts have been directed toward the fabrication of micro- and nano-structural hematite with a controllable size and tailored shape in order to enhance its performance in photocatalysis and other applications. Much work has demonstrated that some delicate nanostructures, especially hollow structures, could effectively alleviate the above mentioned drawbacks since they often exhibited a high light harvesting efficiency and a fast motion of charge carriers.[4] For example, we have demonstrated previously that hollow cocoon-like hematite nanostructures showed high photocatalytic activities in the degradation of methyl orange.[5] Although great successes have been achieved in the fabrication of hollow α-Fe_2O_3 structures, the synthesis of non-spherical hollow structures still remains a big challenge.[5–8] And more importantly, the advantage of hollow structures has rarely been carefully investigated.[9] In previous reports, hollow structures showed enhanced photocatalytic activities when comparing with nanoparticles. However, the structures of these two categories are quite different from each other, making it difficult to identify the beneficial effects of hollow structures. Therefore, it is highly desirable to fabricate materials with different hollowness but similar shapes and investigate the advantage of the hollow structures.

Besides hollow structures, porous structures have also been considered as a promising candidate for photocatalysis. For example, Cao *et al.* demonstrated that mesoporous hematite microspheres showed high photocatalytic activities in the degradation of salicylic acid.[10] Similar to hollow structures, although porous structures have been intensively studied, the in-depth understanding of their beneficial effects is still needed. The difficult part is to produce samples with similar morphologies but different porosities. To this end, Lou and co-workers demonstrated a selective etching method to fabricate α-Fe_2O_3 microparticles with tunable porosity.[11] Wang and co-workers demonstrated the controlled synthesis of porous α-Fe_2O_3 using a similar method.[12] However, this method requires accurate control of experimental parameters and suffers from tedious procedures. Thus, it is urgent to develop a facile and feasible approach for the preparation of porous structures.

Herein, we report a facile hydrothermal method to synthesize spindle-like α-Fe_2O_3 nanostructures. By simply adjusting the concentrations of raw materials and the reaction temperature, α-Fe_2O_3 nanospindles with tunable hollowness and porosity could be readily obtained. In particular, three samples, namely α-Fe_2O_3 nanospindles with a solid interior, α-Fe_2O_3 nanospindles with a hollow interior, and porous α-Fe_2O_3 nanospindles with a hollow interior were prepared. These three samples of similar sizes were then evaluated as catalysts for the photodegradation of Rhodamine B (RhB). By comparing their performances, we are able to get a better understanding of the advantages of hollow and porous structures.

[a] *College of Chemistry and Chemical Engineering, Xiamen University, Xiamen, China. E-mail: zcwang@xmu.edu.cn; Fax: +86 592 2180728; Tel: +86 592 2180728*
[b] *College of Materials, Xiamen University, Xiamen, China*

† Electronic supplementary information (ESI) available. See DOI: 10.1039/c3ce41899e

The results show that the porous hollow structures exhibited highest photocatalytic activity.

In a standard synthesis of the α-Fe_2O_3 nanospindles, a mixture of $FeCl_3{\cdot}6H_2O$, $NH_4H_2PO_4$ and Na_2SO_4 was kept at 180–210 °C under hydrothermal conditions for 48 h. Fig. 1 shows the scanning electron microscopy (SEM) and transmission electron microscopy (TEM) images of the sample (denoted as sample A) prepared with 7.5×10^{-4} M $NH_4H_2PO_4$ after a hydrothermal reaction at 180 °C for 48 h. It can be seen that the product is composed of spindle-like nanoparticles. The corresponding selected area electron diffraction (SAED) pattern (Fig. 1d) of an individual nanospindle (Fig. 1c) clearly reveals the single-crystal nature of the product. The high-resolution TEM (HRTEM) image (Fig. 1e) taken from the area marked by a square in Fig. 1c indicates the high-crystalline nature of the α-Fe_2O_3 nanospindles. The lattice fringes are clear and highly visible with a spacing of 0.46 nm, corresponding to the distance of the {0003} planes of α-Fe_2O_3. Statistical analysis of particle dimensional distributions based on TEM indicates that the as-obtained nanospindles have diameters of *ca.* 98 nm and lengths of *ca.* 440 nm.

By simply varying the concentration of $NH_4H_2PO_4$ and the reaction temperature, α-Fe_2O_3 nanospindles with a hollow interior (denoted as sample B) could be obtained. Fig. 2 shows the SEM and TEM images of the product obtained with 7.5×10^{-4} M $NH_4H_2PO_4$ after a hydrothermal reaction at 210 °C for 48 h. Some broken holes can be seen clearly in Fig. 2a–c, suggesting the sample exhibits a similar spindle-like shape to sample A but with a hollow interior. An analysis of the SAED pattern indicates that the diffraction spots can be assigned to the (01–12) and (0–114) planes. Fig. 2e shows the HRTEM image of the area marked by a square in Fig. 2c. The inter-plane distance is scaled to be 0.37 nm, which matches the inter-plane distances of the {01–12} planes and is also consistent with the SAED pattern. The typical size of the hollow nanospindles is 98 nm in diameter and 460 nm in length and the thickness of the shell is 18 nm. Samples A and B can be considered as a pair of parallel subjects since their sizes and shapes are very similar to each other and the only difference between these two samples is the hollowness. Therefore, it will be helpful to intuitively understand the beneficial effect of hollow structures by comparing their photocatalytic activities.

Besides hollow structures, porous structures are also of great interest. Interestingly, when a certain amount of Na_2SO_4 was introduced to our system, porous α-Fe_2O_3 nanospindles with a hollow interior (denoted as sample C) could be readily obtained. Fig. 3 shows the SEM and TEM images of the product obtained with 5.5×10^{-3} M Na_2SO_4 and 7.5×10^{-4} M $NH_4H_2PO_4$ after a hydrothermal reaction at 200 °C for 48 h. The porous structure can be seen from the SEM images (Fig. 3a and b). When viewed under a TEM, a distinct hollow interior and hierarchical shell can be clearly identified (Fig. 3c). From close observation, it can be found that the shell of the product is composed of nanoparticles (Fig. 3d). From the HRTEM image (Fig.3e), the lattice fringes are measured to be 0.37 nm, which is in agreement with the {01–12} lattice spacing of rhombohedral hematite. Fig. 3f shows the corresponding SAED pattern, confirming the single-crystal nature of the particular subunits. The size of sample C is 390 nm in length and 110 nm in diameter. Although the size of sample C is a little different from those of samples A and B, it is still helpful to understand the advantage of porous structures since sample C also exhibits a spindle-like shape. In a word, by simply adjusting the experimental parameters, the hollowness and porosity of α-Fe_2O_3 nanospindles can be readily tuned. The N_2 sorption measurements (Fig. S1, see ESI†) further

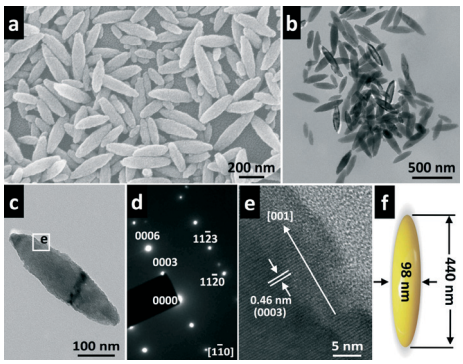

Fig. 1 (a) SEM, (b and c) TEM images, (d) corresponding SAED pattern, (e) HRTEM image and (f) structural model of the as-obtained α-Fe_2O_3 nanospindles with a solid interior.

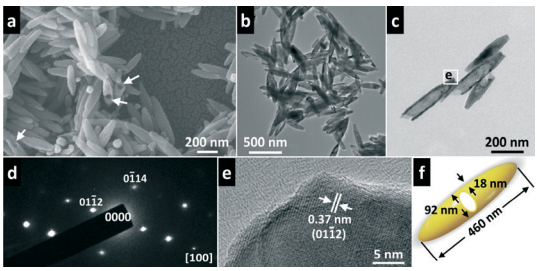

Fig. 2 (a) SEM, (b and c) TEM images, (d) corresponding SAED pattern, (e) HRTEM image and (f) structural model of the as-obtained α-Fe_2O_3 nanospindles with a hollow interior.

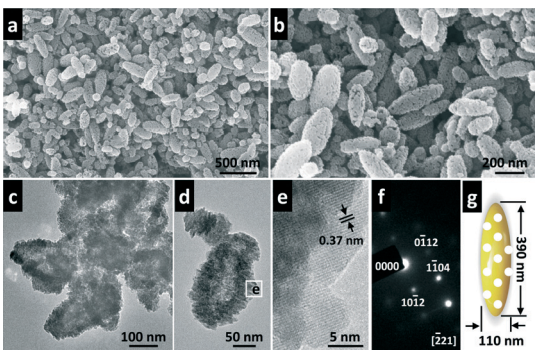

Fig. 3 (a and b) SEM, (c and d) TEM and (e) HRTEM images, (f) corresponding SAED pattern and (g) structural model of the as-obtained α-Fe_2O_3 porous nanospindles with a hollow interior.

confirm that the surface areas and pore-distributions varied from sample A to sample C (Table 1). The structures of the obtained samples A, B and C were characterized using X-ray diffraction (XRD). For all samples, the diffraction peaks are in good agreement with those of hematite (JCPDS card no. 33-0664), suggesting the obtained samples have a trigonal iron oxide structure ($R\bar{3}c$) with high purity (Fig. 4).

Based on experimental results and the literature,[13–17] a possible formation mechanism of the products was proposed. As we know, phosphate ions have been widely used as a shape controller to induce anisotropic growth of hematite nanocrystals.[13–17] They can selectively adsorb on the (11–20) and (10–10) planes and consequently restrict the growth of these planes.[13] On the other hand, the adsorption capacity and affinity for phosphate to the hematite (0001) planes are very weak.[17] Therefore, in the presence of phosphate ions, the α-Fe_2O_3 nanocrystals would grow along the [001] direction, leading to the formation of spindle-like structures (sample A). While under acidic conditions (due to the presence of $NH_4H_2PO_4$) at high reaction temperatures (*e.g.* 210 °C), the nanoparticles may begin to dissolve by the attacking of protons [eqn (1)]. Moreover, the phosphate ions can promote dissolution by their coordination effect with detached ferric ions [eqn (2)].[17] This dissolution process may also accompany a recrystallization process, resulting in the formation of hollow nanospindles (sample B). For sample C, a high concentration of $NH_4H_2PO_4$ and extra Na_2SO_4 were used. The high concentration of phosphate ions helps to keep the (0001) anisotropy, maintaining the spindle-like shape of sample C. Meanwhile, the sulfate ions can also accelerate the dissolution of α-Fe_2O_3 nanoparticles [eqn (3)]. And the dissolving rate is much faster than that of sample B due to the strong ability of sulfate ions in coordinating with Fe^{3+} ions.[17] In this case, the inside-out dissolution may be non-uniform. The recrystallization process may also occur at this stage. As a result, hollow nanospindles with porous structures were formed.

$$Fe_2O_3 + 6H^+ \rightarrow 2Fe^{3+} + 3H_2O \quad (1)$$

$$Fe^{3+} + xH_2PO_4^- \rightarrow [Fe(H_2PO_4)_x]^{3-x} \quad (2)$$

$$Fe^{3+} + xSO_4^{2-} \rightarrow [Fe(SO_4)_x]^{3-2x} \quad (3)$$

The three samples were then used as catalysts for the photo-degradation of RhB. Fig. 5a shows the changes of the RhB relative concentrations (C/C_0) as a function of irradiation time, where C is the concentration of RhB at the irradiation time t and C_0 is the initial concentration. For comparison, the photodegradation of RhB without a catalyst has also been performed and the result shows that the self-degradation of RhB is almost negligible. When α-Fe_2O_3 nanoparticles are used under the same conditions, the photodegradation rates of RhB are significantly increased. In addition, the photocatalytic activities of samples A–C are found to follow the sequence of A < B < C. For example, sample B shows a much higher activity than sample A under visible light irradiation. Nearly 37% of RhB is degraded in 150 min by sample B, resulting in a high reaction rate constant of $k_B = 0.0034\ min^{-1}$, while only 25% of RhB can be degraded by sample A, corresponding to a reaction rate constant $k_A = 0.00193\ min^{-1}$. In previous studies, hollow structures often exhibited higher photocatalytic activities when comparing with nanoparticles. For example, Li *et al.* found that hollow Fe_2O_3 spheres showed a higher activity than ring-like nanocrystals.[18] However, these two samples can hardly be considered as a pair of parallel subjects since they present not only a difference in hollowness but also in size and shape. This makes the investigation of the advantage of hollow structures become quite difficult. In this work, samples A and B are of a similar size and spindle-like shape and the only difference between them is the hollowness. Therefore, the hollow structures must be responsible for their different performances in the photodegradation of RhB. This structure-dependent property is confirmed by the results of the N_2 adsorption measurements. As shown in Table 1, the specific surface area (19.9 $m^2\ g^{-1}$) of sample B is higher than that of sample A (14.3 $m^2\ g^{-1}$). The high surface area of sample B results in more unsaturated surface coordination

Table 1 Key parameters of samples A, B and C

Sample	Surface area ($m^2\ g^{-1}$)	Total pore volume ($cm^3\ g^{-1}$)	Average pore size (nm)
A	14.3	0.037	7.48
B	19.9	0.053	9.14
C	30.4	0.092	15.21

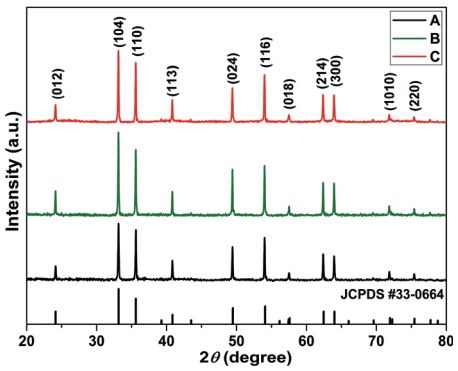

Fig. 4 XRD patterns of the as-prepared samples A, B and C.

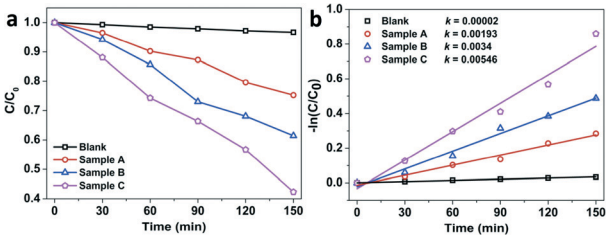

Fig. 5 (a) Photodegradation of RhB using different catalysts under visible light irradiation. (b) Comparison of the apparent reaction rate constant (k), assuming the reactions follow the pseudo-first-order.

sites and thus would adsorb more molecules. Meanwhile, the hollow interior allows efficient transport of the reactant molecules, leading to a higher photodegradation efficiency. Furthermore, multiple reflections of the irradiation light may occur in the hollow interior, resulting in more efficient absorption of light.[19] Analogously, since samples B and C have similar hollow spindle-like morphologies but different porosities, it is possible to get an intuitive understanding of the beneficial effect of porous structures by comparing their performances. As shown in Fig. 5, about 58% of RhB can be degraded in the presence of sample C, which is significantly higher than that of sample B. Two reasons may account for the better ability of sample C. One is the higher absorption capacity. More active sites that are essential for catalytic reactions can be generated by the pores (the total pore volume and average pore diameter of sample C are much higher than those of sample B, Table 1). Therefore, more RhB molecules can be adsorbed on the surfaces. Another reason is that the porous structure can effectively separate the photoinduced electron–hole pairs. The holes can readily migrate to the surface and oxidize RhB. As a result, a better performance of sample C can be achieved.

In summary, α-Fe_2O_3 nanostructures with similar spindle-like shapes but different hollowness and porosities have been synthesized by a facile hydrothermal method. Three samples, namely α-Fe_2O_3 nanospindles with a solid interior (sample A), α-Fe_2O_3 nanospindles with a hollow interior (sample B) and porous α-Fe_2O_3 nanospindles with a hollow interior (sample C) were prepared and evaluated as photocatalysts for the degradation of RhB. The results show that sample C exhibits the highest activity among the three samples. This work presents an intuitive understanding of the beneficial effects of hollow and porous structures.

Experimental section

Materials preparation

The α-Fe_2O_3 nanocrystals were synthesized by a modified hydrothermal method.[13] Briefly, $FeCl_3{\cdot}6H_2O$ was dissolved in 80 mL of deionized water, then a certain amount of $NH_4H_2PO_4$ was added to the solution followed by ultrasonic treatment for 5 min. The final concentrations of the raw materials were 0.02 M for $FeCl_3{\cdot}6H_2O$ and 7.5×10^{-4} M for $NH_4H_2PO_4$. The mixture was then transferred into a 100 mL autoclave, sealed and maintained at 180 °C for 2 d. After the mixture was cooled to room temperature naturally, the product was centrifuged and washed, and finally dried at 60 °C for 12 h to get the α-Fe_2O_3 nanospindles with a solid interior. The synthetic procedure for hollow α-Fe_2O_3 nanospindles was the same as that of α-Fe_2O_3 nanospindles except that the concentration of $NH_4H_2PO_4$ was adjusted to 6.0×10^{-4} M and the reaction temperature was raised to 210 °C. For the porous α-Fe_2O_3 nanospindles with a hollow interior, Na_2SO_4 with a concentration of 5.5×10^{-3} M and $NH_4H_2PO_4$ with a concentration of 9.0×10^{-4} M were added to 80 mL of 0.02 M $FeCl_3{\cdot}6H_2O$ solution followed by hydrothermal treatment at 200 °C for 2 d.

Materials characterization

The phase and morphology of the products were characterized by X-ray diffraction (XRD, Philips, X'pert PRO) with Cu Kα radiation, scanning electron microscopy (SEM, LEO 1530), and transmission electron microscopy (TEM, JEOL JEM-2100). The surface area, pore volume and pore size of the catalysts were calculated by N_2 adsorption–desorption isotherms using a TriStar 3000 with the Brunauer–Emmett–Teller (BET) and Barrett–Joyner–Halenda (BJH) methods.

Photocatalytic measurements

The photocatalytic activity of the catalysts was evaluated by the visible-light photo-degradation of Rhodamine B (RhB). In a typical test, 100 mg of the α-Fe_2O_3 nanocrystals were added to 100 mL of 20 mg L^{-1} RhB solution. The suspension was stirred in the dark for 40 min to reach absorption equilibrium and then irradiated using a photochemical reactor (visible-light 420 nm, NBET HSX-F300, Beijing) under continuous stirring. Analytical samples were taken from the reaction suspension after various reaction times and centrifuged to remove the particles for analysis. UV-vis adsorption spectra were recorded at different intervals to monitor the degradation process using a Shimadzu 2550 spectrophotometer.

Acknowledgements

The authors thank the State Key Development Program for Basic Research of China (grant no. 2007CB935603) and the National Natural Science Foundation of China (grant no. 51372212) for financial support.

Notes and references

1 C. M. Eggleston, *Science*, 2008, **320**, 184.
2 K. Sivula, F. Le Formal and M. Grätzel, *ChemSusChem*, 2011, **4**, 432.
3 Y. Cui and C. M. Lieber, *Science*, 2001, **291**, 851.
4 S. Nishimura, N. Abrams, B. A. Lewis, L. I. Halaoui, T. E. Mallouk, K. D. Benkstein, J. Van de Lagemaat and A. J. Frank, *J. Am. Chem. Soc.*, 2003, **125**, 6306.
5 H. Liang and Z. Wang, *Mater. Lett.*, 2013, **96**, 12.
6 Z. Wang and X. W. Lou, *Adv. Mater.*, 2012, **24**, 4124.
7 Z. Wang, D. Luan, C. M. Li, F. Su, S. Madhavi, F. Y. C. Boey and X. W. Lou, *J. Am. Chem. Soc.*, 2010, **132**, 16271.
8 Z. Wang, D. Luan, S. Madhavi, C. M. Li and X. W. Lou, *Chem. Commun.*, 2011, **47**, 8061.
9 B. Wang, J. S. Chen and X. W. Lou, *J. Mater. Chem.*, 2012, **22**, 9466.
10 S. W. Cao and Y. J. Zhu, *Nanoscale Res. Lett.*, 2011, **6**, 1.
11 J. S. Chen, T. Zhu, X. H. Yang, H. G. Yang and X. W. Lou, *J. Am. Chem. Soc.*, 2010, **132**, 13162.
12 D. Su, H. S. Kim, W. S. Kim and G. Wang, *Microporous Mesoporous Mater.*, 2012, **149**, 36.

13 M. Ozaki, S. Kratohvil and E. Matijevic, *J. Colloid Interface Sci.*, 1984, **102**, 146.
14 T. Sugimoto, A. Muramatsu, K. Sakata and D. J. Shindo, *J. Colloid Interface Sci.*, 1993, **158**, 420.
15 M. Ocaña, M. P. Morales and C. J. Serna, *J. Colloid Interface Sci.*, 1995, **171**, 85.
16 C. J. Jia, L. D. Sun, Z. G. Yan, L. P. You, F. Luo, X. D. Han, Y. C. Pang, Z. Zhang and C. H. Yan, *Angew. Chem.*, 2005, **117**, 4402.
17 C. J. Jia, L. D. Sun, F. Luo, X. D. Han, L. J. Heyderman, Z. G. Yan, C. H. Yan, K. Zheng, Z. Zhang, M. Takano, N. Hayashi, M. Eltschka, M. Kläui, U. Rüdiger, T. Kasama, L. Cervera-Gontard, R. E. Dunin-Borkowski, G. Tzvetkov and J. Raabe, *J. Am. Chem. Soc.*, 2008, **130**, 16968.
18 L. Li, Y. Chu, Y. Liu and L. Dong, *J. Phys. Chem. C*, 2007, **111**, 2123.
19 M. Tadic, N. Citakovic, M. Panjan, B. Stanojevic, D. Markovic, Đ. Jovanovic and V. Spasojevic, *J. Alloys Compd.*, 2012, **543**, 118.